We are IntechOpen, the world's leading publisher of Open Access books Built by scientists, for scientists

6,900
Open access books available

185,000
International authors and editors

200M
Downloads

Our authors are among the

154
Countries delivered to

TOP 1%
most cited scientists

12.2%
Contributors from top 500 universities



WEB OF SCIENCE™

Selection of our books indexed in the Book Citation Index in Web of Science™ Core Collection (BKCI)

Interested in publishing with us?
Contact book.department@intechopen.com

Numbers displayed above are based on latest data collected.
For more information visit www.intechopen.com



Chapter 4

Texturing Tendency in β-Type Ti-Alloys

Mohamed Abdel-Hady Gepreel

Additional information is available at the end of the chapter

http://dx.doi.org/10.5772/53588

1. Introduction

1.1. Textures

Preferred orientation of crystal is an intrinsic feature of metals and has an influence on physical properties such as strength, electrical conductivity and wave propagation, particularly in the anisotropy of these properties [1]. For example, in the single crystals of many metals it is well known that the main mechanism of plastic deformation, on a microscopic scale, is a simple shear parallel to certain planes and directions. Slip will occur in a certain direction on a crystallographic plane when the shear stress in that direction attains a critical value [2]. So, the observed strength might depend on the loading direction of the crystal. Some other physical properties of the crystal vary depending on the measuring direction.

On the other hand, in a polycrystalline metal, each grain normally has a crystallographic orientation different from that of its neighbors resulting in isotropy of the properties of the metal. Considering a polycrystalline as a whole, the orientations of the grains may tend to cluster about some particular orientations. Such polycrystalline is said to have a preferred orientation, or texture, which may be defined simply as anon-random distribution of crystal orientations [3]. In this case, a polycrystalline performs in a way close to the single crystal depending on the strength of texture formed in it.

The appearance of preferred orientations (or texture) is very common. The texture produced by forming such as wire drawing and rolling, is called a deformation texture. The grains in a polycrystalline metal tend to rotate during plastic deformation, which results in the texture formation. Each grain undergoes slip and rotation in a complex way by the imposed force and by the restriction of slip and rotation of adjoining grains [3]. The preferred orientation also appear when cold-worked metal (show a deformation texture) is annealed. This is the so-called recrystallization texture (or annealing texture).

INTECH
open science | open minds

© 2013 Gepreel; licensee InTech. This is an open access article distributed under the terms of the Creative Commons Attribution License (http://creativecommons.org/licenses/by/3.0), which permits unrestricted use, distribution, and reproduction in any medium, provided the original work is properly cited.

Texture may be influenced by a number of factors that can be divided into two major categories, material variables and process variables [4]. The material variables include crystal structure, solute content, second-phase particles, and initial grain size. The process variables include the amount of deformation, strain rate, stress and strain states [5], reduction in thickness and area, intermediate annealing conditions, heating and cooling rates, and annealing atmosphere [6].

1.2. Texture characterization techniques

The most common method of characterizing texture is the presentation of pole figures where X-ray diffraction is used to specify the orientation of the crystallographic planes in space using the stereographic projection. The two different representations of these textures are the inverse and direct pole figures [1]. The pole figure is a two-dimensional projection of the three-dimensional distribution and represents the probability of finding a pole to a lattice plane (*hkl*) in a certain sample direction. Pole figures are normalized to express this probability in multiples of a random distribution. Inverse pole figures are also projections of the orientation distribution factor (ODF), but in this vase the probability of finding a sample direction relative to crystal directions is plotted. In other words, the difference between these two representations is their reference frame; inverse pole figures are shown with respect to the specimen reference frame, while direct pole figures refer to the crystal reference frame [1].

Local orientation can also be measured with the Scanning Electron Microscope (SEM). Interaction of the electron beam with the uppermost surface layer of the sample produces electron back-scatter diffraction patterns (EBSPs or EBSD) that are analogous to kikuchi patterns in Transmission Electron Microscope (TEM). EBSD are captured on a phosphorus screen and recorded with a low intensity video camera or a CCD device [1].

The texture of sheet is in the most highly developed form, so, most of grains are oriented and the sheet surface becomes roughly parallel to a certain crystallographic plane (hkl). Also, a certain direction [uvw] in that plane becomes roughly parallel to the direction of deformation. Such a texture is described by the shorthand notation (hkl)[uvw], and is called an ideal orientation. Most sheet textures, however, have so much scatter in orientations, and hence they may be approximated symbolically only by the sum of number of ideal orientations or texture components [3].

1.3. Texture types

1.3.1. Deformation texture

The deformation of a polycrystal is a very complicated heterogeneous process. When an external stress is applied to the polycrystal, it is transmitted to individual grains. Dislocations move on slip systems, dislocations interact and cause 'hardening', grains change their shape and orientation, thereby interacting with neighbours and creating local stresses that need to be accommodated [1].

The weakest slip systems in fcc metals are{111}<110>, consisting of 12 symmetrically equivalent variants. Activity of these systems produce a characteristic texture pattern during rolling [1]. The large number of slip systems makes it easy to achieve compatibility and the rolling texture can be well explained with the Taylor theory, especially if individual slip systems are allowed to harden, according to their activity [8] and if allowance is made for some heterogeneity across small grain boundaries [9].

Also, the bcc metals have 12 variants of slipping system [1] and the most common deformation mode in bcc metals is {110}<111> slip, which is a transposition of slip plane and slip direction with respect to fcc metals. Also, bcc metals slip on other planes than {110} in the <111>direction [10] such as {112}<111>and {123}<111> [3]. Generally, the most preferred orientations in cold rolled bcc metals consist of two types. The first type is represented by {100}<110> or its rotations around<110> axis, resulting in {hkl}<110>. The other is represented by {111}<112> or its orientations around surface normal axis, resulting in {hkl}<uvw> [3].

1.3.2. Recrystallization texture

The relationship between slip and crystal rotations is straightforward. Other processes such as climb, grain boundary sliding, and diffusion in general may also affect orientation distributions [1]. Of particular importance is recrystallization. Recrystallization is the replacement of deformed grains by the nucleation and growth of recrystallized grains, both can lead to drastic changes in texture. The nuclei during recrystallization are regions exists in the deformed microstructure and at the same time the recrystallization does not lead to precise orientation relationship between deformed and recrystallized grains. Although there might be some approximate orientation relationships present in-between the recrystallized and parent grains, there has been no report in making quantitative predictions for recrystallization texture based on such approximate orientation relationships. The texture evolution is still highly sensitive to almost the entire spectrum of metallurgical variables and sometimes difficult to fully predict. However sometimes it is observed that the recrystallization texture component bear crystallographic relationships to the original deformation textures, which may be described by rotations about simple crystal direction which is often ~25^{o} rotations around <110> directions in bcc alloys [11].

In recrystallization, the nuclei by the shear bands competes with the nuclei forming at other nucleation sites. Since stored energy represents the driving force for recrystallization, certain crystallographic orientations will be enhanced during annealing in comparison with others because of more favorable nucleation and/or growth kinetics [12]. Grains with higher stored energies may be consumed through boundary migration by grains with less stored energy (i.e., growth stage). Alternatively, dislocation-free nuclei may form grains with high dislocation density and then grow at expense of others. The texture which finally forms is believed to be controlled either by nucleation or by grain growth. It is possible that grain growth is 'oriented', i.e. for some reasons grains with certain crystallographic orientation grow faster than others. In that case the grain growth mechanism is likely to control the final texture. Otherwise, 'oriented' nucleation may control the final texture. The texture fresh nuclei may not be random and reflect the final texture. The last

word has not been yet said on this problem. Not only orientation distribution, but also grain size distribution are important considerations [1].

The stored energy is the most important parameter characterizing the influence of microstructure on the recryasallization process which is a driving force of it. The stored energy is proportional to the average critical shear stress for slip in the crystal [13].

1.4. Elastic anisotropy change with β-phase stability

The elastic anisotropy of bcc metals can be represented by the elastic anisotropy factor, A, which is calculated from elastic constants from the formula, $A= C_{44}/C'$. $C'= (C_{11}-C_{12})/2$ represents the resistance for the {110}<110> shear and C_{44} represents the resistance for the {001}<001> shear [13] and both of them increases with β-phase stability [3,10]. Further more, the ideal strength for tension σ_{max}, which is needed for tensile separation of bcc crystal on {100} plane, is proportional to C′ and ideal strength for shear σ_{max} which is needed for plastic shear along <111> on {011}, {112} or {123} [14]. As a result, the deformation mechanism in bcc alloys is related to the β-phase stability as mentioned before [15]. Figure 1 show the change in A and C′ with the Cr-content in Ti-Cr binary alloys. The Cr-content is related to β-phase stability [16]. So, it is expected that the anisotropy and texturing tendency are related to the β-phase stability in β Ti-alloys. So, a correlation between the β-phase stability and the texturing tendency will be presented below.

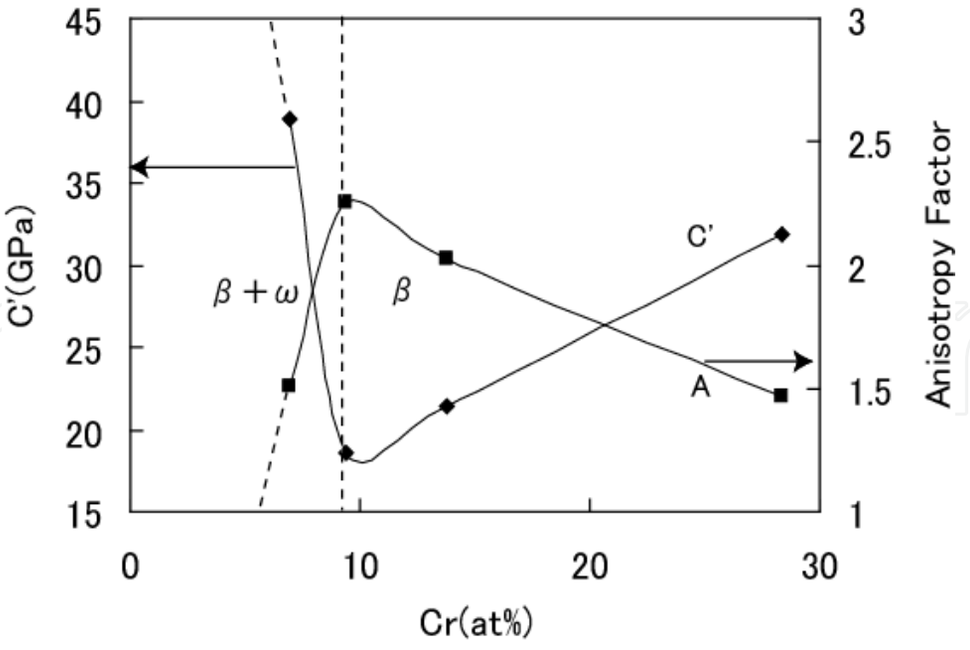


Figure 1. Changes in elastic anisotropy factor, *A*, and tetragonal shear constant, C', with the β –phase stability in Ti-Cr binary alloys. *A* shows maximum and C' shows minimum at the β/β+ω phase boundary

http://dx.doi.org/10.5772/53588

1.5. BCC β-type Ti alloys

Recently, considerable efforts have been devoted to exploring novel β-titanium alloys for different applications because of their superior properties such as the superelasticity, low Young's modulus, high strength-to-weight ratio, and better formability compared to the α and $\alpha + \beta$ titanium alloys [17-20]. The mechanical properties of the β-titanium alloys depend strongly on the presence of several phases (e.g., ω phase and martensitic α"-phase) in them. The appearance of these phases could be controlled by either the optimized alloy design [19,20] or the materials processing [18]. The phases present in the alloy are related to the alloying elements and the thermal history of the alloy. The change of the Ti-alloy type depending on the β-stabilizer content is shown schematically in figure 2.

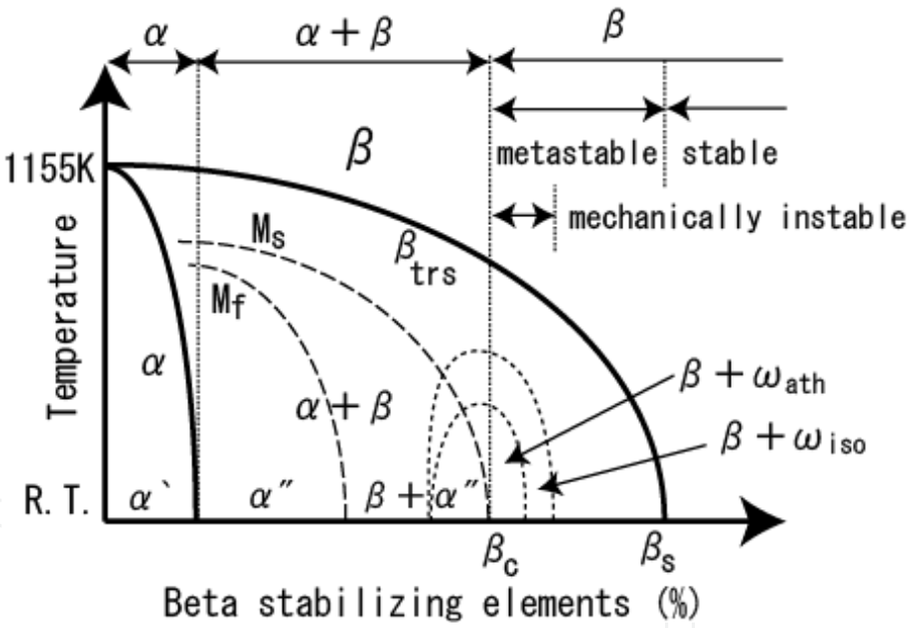


Figure 2. Schematic phase diagram of titanium alloys with the decomposition products of the β-phase. β_c is the critical minimum β stabilizer amount for near β or metastable β alloys to retain β completely on quenching from β phase field and β_s is the minimum amount of β stabilizer for stable β alloys; β_{trs}, M_s and M_f refer to β-transus, martensite start and finish temperatures, respectively.

Most of the β-Ti alloys possess good workability. It is possible to fabricate a cold-rolled sheet of the alloys by a reduction ratio higher than 90%. In this case strong deformation textures are developed and even recrystallization texture may be developed when subsequently heat treated. Therefore, the anisotropy in elastic and plastic properties is induced inevitably to the sheet, resulting in the modification of alloy properties such as the elastic modulus, elastic strain, Poisson's ratio, strength, ductility, toughness, magnetic permeability and the energy of magnetization [21]. In other words, the elastic and plastic properties of the alloy may be improved by using an orientation effect arising from the textures. It is, therefore, important to examine which kind of textures can be developed in the β-Ti alloys under the given conditions of thermo-mechanical treatment, and to investigate the texture effect on the elastic and plastic properties.

In this chapter, the effect of β-phase stability on the texturing tendency of β-type Ti-alloys are discussed. It is important to high light here that Zr has been known for many decades as neutral element on the stability of β-phase; however, the recent studies have proved that Zr shows a β-stabilizing effect in the β-type alloys [20,22]. Therefore, in this study, it was chosen to study two groups of alloys, one group is Zr-free β-type alloys (referred hereafter as A-alloys) and the other group is high Zr-containing alloys (referred herefater as Z-alloys). The design of these alloys is explained below.

2. Alloys design

The two series of alloys were designed across the single β-phase boundary, β/β+ω+(α"), with the aid of the $\overline{Bo}$- $\overline{Md}$ diagram. At this boundary, the elastic anisotropy factor, $A=C_{44}/C'$, is rather high since the value of the elastic shear modulus, $C' = (C_{11}-C_{12})/2$, is diminishing as the alloy approaches this boundary [23,24], as shown in figure 1. Also, it has been reported that the $(C_{11}-C_{12})/2$ is related to the electronic parameter e/a (electron-per-atom ratio) and its value approaches zero when the e/a value is about 4.24 [23]. This is the reason why, in this work, the e/a value was kept at 4.24 in almost all the designed alloys. Here, $\overline{Bo}$is the average bond order between atoms, and $\overline{Md}$is the average d-orbital energy level (eV) of the elements in the alloy.

In A-alloys, A00 alloy is designed to be located in the β+α"(+ω) phase zone in the $\overline{Bo}$-$\overline{Md}$ diagram [20], as shown in figure 3. The composition of A-alloys is listed in table 1. The Fe and O were added to stabilize the β-phase of the alloys. Fe was chosen to stabilize β-phase due to its very strong β-stabilizing effect as obvious from its alloying vector in the $\overline{Bo}$-$\overline{Md}$ diagram [22]. The oxygen was added to the alloys to suppress the ω and martensite phases, as discussed in ref.[20].

As for Z-alloys, four alloys were designed with the aid of the $\overline{Bo}$-$\overline{Md}$ diagram across the β/β +ω+(α") phase boundary in two steps; in the 1st step, four alloys were designed, consist mainly of β-stabilizers, Ta, Nb, Mo, Cr and V. These four alloys are shown across the β/β+ω+ (α") phase boundary with the dashed arrow in figure 3.

http://dx.doi.org/10.5772/53588

As discussed above, Zr works as β-stabilizer in the β-type Ti alloys and also raises the $\overline{Bo}$ value of the alloy. The 2nd step was to add Zr to the alloys with different amounts varies with the required β-phase stability of each alloy. So, the stability difference between the alloys will be much bigger and the properties difference would be clearer. Considering that the e/a value of the alloys did not change after Zr addition.

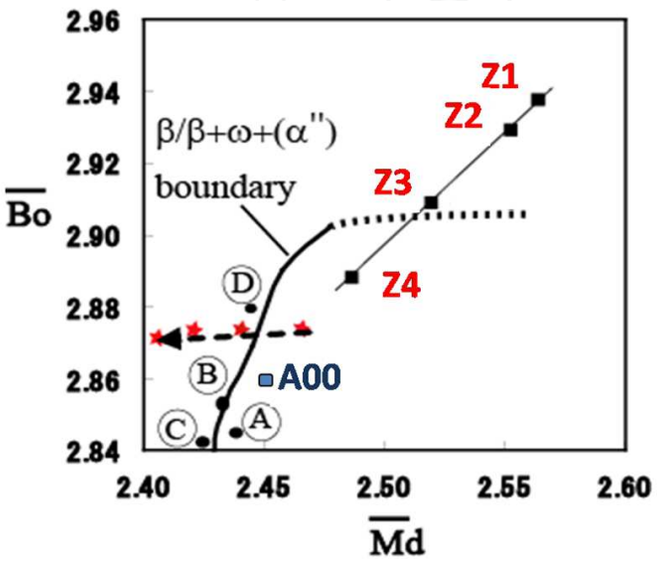


Figure 3. Extended $\overline{Bo}$-$\overline{Md}$ diagram showing the β/β+ω+(α") phase boundary and the location of the designed alloys, A00 and Z1-4. Also, the alloys A, B, C, and D are 35mass%Nb-4mass%Sn, Ti-24Nb-3Al, Ti-35mass%Nb-7.9mass% Sn, and Ti-22Nb-6Ta, respectively.

At last, the four designed Z-alloys, namely Z1 - 4, are located across the β/β+ω+(α") phase boundary in the high $\overline{Bo}$ region (i.e., high Zr-Containing alloys zone) in the extended $\overline{Bo}$-$\overline{Md}$ diagram shown in figure 3, and the chemical compositions are listed in Table 1.

3. Experimental procedure

As explained above, two series of alloys, namely; high Zr-containing [Z-alloys] and Zr-free [A-alloys], were designed across the β/β+ω+(α") phase boundary and the chemical compositions are listed in table 1. In this chapter, all the compositions are given in atomic percent units unless otherwise noted. These alloys were prepared by the arc-melting of an appropriate mixture of pure metals (purity: 99.99%) under a high purity argon gas atmosphere. The button-shaped specimens with average 7.5 mm in thickness were cut and homogenized at 1273K for 7.2ks, and then cold rolled to the plate with 4.5 mm thick, followed by the solution treatment at 1223K for 1.8 ks. Subsequently, the specimen was cold rolled by 60%, 90 % or 98% reduction in thickness. The cold rolled specimen is called CR specimen hereafter. The 90%CR specimen was then solution-treated at 1223K for 1.8ks. This finally solution treated specimen is called ST specimen hereafter.

The phases existing in the specimen and its pole figures were identified by the conventional X-ray diffraction (XRD) using a Ni-filtered Cu-Kα radiation. Electron back scattered diffraction (EBSD) analysis was also made using a HITACHI S-3000H scanning electron microscope (SEM) equipped with a OXFORD INCA Crystal EBSD detector, operated at an acceleration voltage of 20 kV and a tilt angle of 71°. The microstructural characterization was performed using the optical microscope (OM), the scanning electron microscope (SEM) and the transmission electron microscopy (TEM).

Alloy	O	Fe	V	Cr	Mo	Nb	Ta	Zr
Z1			4		2	9	7	30
Z2					3	15	3	25
Z3				1		8	14	15
Z4						4	20	5
A00						17	6	
A01	1					17	6	
A11	1	1				17	6	

Table 1. Chemical compositions of the designed A and Z-alloys, at.%.

4. Results and discussion

4.1. Change in β-phase stability with alloys' composition

The β-phase stability increases with increasing content of the β-stabilizing elements. Shown in figure 4.a are the X-ray diffraction patterns taken from the A-alloys in the ST condition. The α" martensite phase is the predominant phase in A00 alloy beside small amount of β and ω phases. The α" martensite phase is suppressed by O addition to the A00 β-phase alloys. As shown in figure 4.a, the addition of 1 mol.% O to A00 alloy was very effective in suppressing the α" martensite phase as observed in A01 alloy. Also, it is clear from this figure that the addition of Fe to the A01 alloy resulted in stabilizing the β-phase as observed in the A11 alloy and the α" martensite phase couldn't be observed by XRD at room temperature.

It can be deducted from the XRD results that the A11 is a single β-phase alloy. So, the least stable single β-phase alloys in the A series is A11 alloy. It is concluded that the co-addition of Fe and O to these β-type alloys is very effective in suppressing the α" martensite phase and instantaneously stabilize β-phase of the alloy. An important observation from figure 4.a is that, the co-addition of only 1% O and 1% Fe could modify greatly the phase stability of alloy A00, with the α" predominant phase, to alloy A11, with the single β-phase. Therefore, the β-phase stability in these alloys increases in the order, A11> A01> A00.

http://dx.doi.org/10.5772/53588

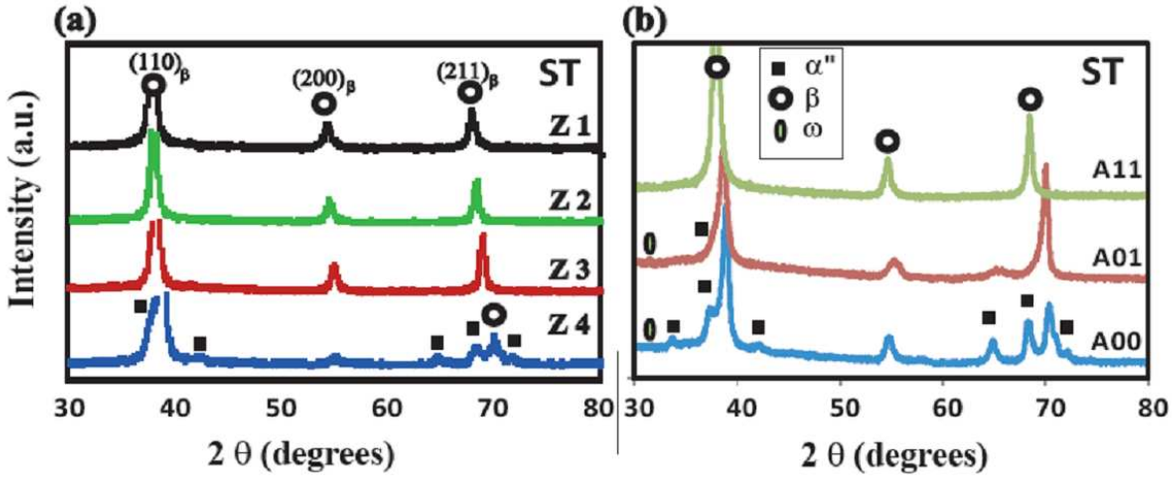


Figure 4. XRD profiles of the alloys Z1-4 (a), and A-alloys (b) in the solution treated at 1223K, ST, after 90% cold rolling.

	Z-alloys (60%CR)				A-alloys (90%CR)		
	Z1	**Z2**	**Z3**	**Z4**	**A00**	**A01**	**A11**
CR, $I_{Rcr}= I_{\{200\}\beta} / I_{\{110\}\beta}$	1.7	1.2	0.8	0.1	0.086	0.194	1.232
ST, $I_{Rst(1)}= I_{\{110\}\beta} / I_{\{200\}\beta}$	6.0	8.6	8.5	33.0			
ST, $I_{Rst(2)}= I_{\{211\}\beta} / I_{\{200\}\beta}$	1.6	2.0	2.2	3.6			

Table 2. X-ray peak intensity ratios of Z-alloys and A-alloy in the CR and ST conditions.

By the same way for Z-alloys, shown in figure 4.b are the X-ray diffraction patterns taken from the Z-alloys in the ST condition. A single β-phase was predominant in the alloys Z1, Z2, and Z3. Only in the alloy Z4, the martensite α''-phase coexisted with the β-phase, as shown in figure 4.b. Therefore, theβ/β+α'' boundary shown in figure 3 is located between the alloys Z3 and Z4 as indicated by a dotted curve. So, the alloy Z3 is the least stable single β-phase alloy which is defined as the alloy containing a least amount of the β-stabilizing elements to get a β single phase [20,25]. According to the $\overline{Bo}$-$\overline{Md}$ diagram shown in figure 3, the alloy closer to the β/β+α'' boundary has the lower β-phase stability, so the β-phase stability in these alloys decreased in the order, Z1> Z2> Z3> Z4. The stability was highest in the alloy Z1 and lowest in alloy Z4.

4.2. Textures developed by cold rolling

Most of the annealed β-type Ti-alloys have random equiaxed grains and their X-ray peak intensity of the $\{110\}_\beta$ plane is the highest among the different atomic planes reflections. However, the $\{100\}_\beta$<110> rolling texture is formed normally after high reduction ratio of the β-type Ti-alloys due to dislocation slipping and grains rotation. In this cold rolling texture, the $\{200\}_\beta$ planes aligned parallel to the rolling plane preferentially. Figure 5.a shows the X-ray

diffraction patterns taken from the Z-alloys in the 60% cold rolled (60CR) condition. It is known that the cold rolling texture is formed in conventional β- type Ti alloys. As a result, the measured X-ray peak intensity ratio of the cold rolled specimen, $I_{Rcr,}$ defined as I_{Rcr}= $I_{\{200\}\beta}$ / $I_{\{110\}\beta}$, changed with cold rolling. Here, $I_{\{200\}\beta}$ and $I_{\{110\}\beta}$ are the X-ray peak intensities of the $\{200\}_\beta$ and $\{110\}_\beta$ reflections, respectively. The I_{Rcr} usually increases with the reduction ratio of cold rolling. In addition, as is evident from figure 5.a and table 2, when the alloys were cold rolled by 60%, I_{Rcr} tended to increase with increasing β-phase stability. In other words, a cold rolling texture was developed in the way that the {200} planes were aligned parallel to the rolling plane preferentially. This texture was formed more readily in the order, Z1>Z2> Z3> Z4, in agreement with the order of the β- phase stability.

Figure 6 (a-c) shows {200}, {110} and {112} pole figures obtained from a 90% cold rolled (CR) specimen of the alloy Z2. The center of the pole figures corresponds to the direction normal to the specimen surface (ND). The right and the top of the pole figures correspond to the rolling direction (RD) and the transverse direction (TD), respectively. It was realized from these pole figures that typically {100}<110> rolling texture with a strength of 97.5 times larger compared to the random orientation is well developed in the 90% cold rolled (CR) specimen of the alloy Z2, as shown in the {100}<110> texture stereoprojection [26] in figure 6 (d). It is important to mention here that the alloy Z2 with the relatively high β-phase stability shows the{100}<110> texture after 90%CR more remarkably, as compared to the lower β-phase stability alloy undergone by the same or even severer cold rolling [18,27,28].

It has been reported that the {100}<110> texture is a main rolling texture formed in the β-type Ti-alloys [17,18,26-28]. Beside this texture, the {211}<110> texture forms in a Ti-35mass %Nb-4mass%Sn alloy [18,26] (location A in figure 3) or the {111}<112> texture forms in a Ti-24Nb-3Al alloy [26] (location B in Figure 3). With a little increase in the β-phase stability, the {100}<110> texture becomes dominant as observed in a Ti-35mass%Nb-7.9mass% Sn alloy [28] (location C in figure 3). As explained in Ref. [20], both Al and Sn work as the β-stabilizing elements in these β-phase alloys. In the much higher β-phase stability alloys such as Ti-22Nb-6Ta alloy (location D in figure 3), only the {100}<110> texture is developed after 99% cold rolling [27]. This was consistent with the present results that the $I_{Rcr,}$ which represents {100}<110> texture, increases monotonously with the β-phase stability. Therefore, it can be concluded that the {100}<110> rolling texture is developing in β-type Ti-alloys and its strength is increasing monotonously with increasing β-phase stability. However, in Ti alloys with low β-phase stability, other rolling textures such as {211}<110> and {111}<112> textures are developing more readily than {100}<110> texture in such low β stability alloys.

In the same way for A-alloys, as is evident from figure 5.b and table 2, when the A-alloys were cold rolled by 90%, I_{Rcr} tended also to increase with increasing β-phase stability. In other words, a rolling texture was developed, in the higher β-phase stability alloys, in the way that the {200} planes aligned parallel to the rolling plane preferentially, in accordance with that reported for the above Z-alloys. For example, the I_{Rcr} of A11 alloy is around 6 times of that of A01 alloy with relatively lower β-phase stability. However, I_{Rcr} (A01) / I_{Rcr} (A00) are around 2 times only. This can be interpreted as the addition of 1% O is less efficient to highly stabilize β-phase and therefore to develop the {100}<110> rolling texture if compared with

http://dx.doi.org/10.5772/53588

the addition of 1% Fe in this A-alloy. However, the O addition seems to be very effective in suppressing the ω- and the α"-phases (in other words, stabilizing β-phase at room temperature), as shown in figure 5.b. It is well know that Fe is very strong β-stabilizer. Therefore, the co-addition of O and Fe in A11 alloy was enough to increase the β-phase stability to a level high enough to develop strong {100}<110> rolling texture, same as in Z-alloys with higher β-phase stability such as Z2 and Z3 alloys, as shown in figure 5.b and table 2.

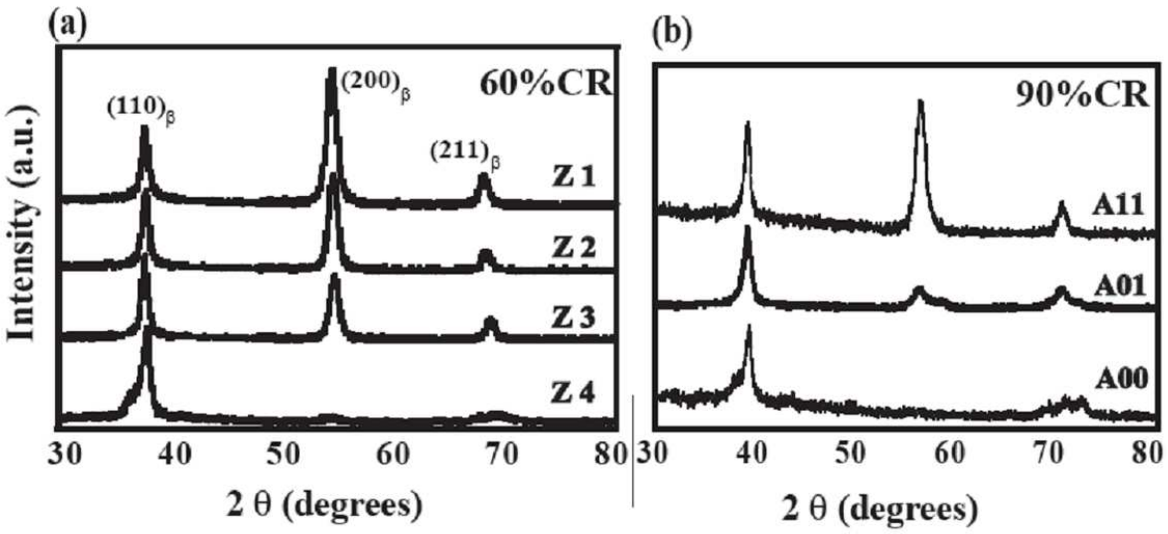


Figure 5. XRD profiles of Z-alloys after 60%CR, (a) and A-alloys after 90%CR, (b).

Figure 7 (a-c) shows {200}, {110} and {112} pole figures obtained from a 98% cold rolled (CR) specimen of the A01 alloy. The center of the pole figures corresponds to the direction normal to the specimen surface (ND). It seems from these pole figures that the {111}<112> rolling texture was developed predominantly compared to the other textures and random grains orientations. The {111}<112> rolling texture developed in A01 after 98%CR is moderate in strength if compared to that {100}<110> rolling texture developed in Z2 alloy after only 90%CR as evidenced from the inverse pole figures shown in Figure 8. This means that the rolling textures in β-type Ti-alloys become stronger with increasing the β-phase stability irrelative to the type of texture developed in them. Also, Z2 with the relatively high β-phase stability shows the{100}<110> texture after 90%CR more remarkably when compared to the lower β-phase stability alloys undergone by the same or even severer cold rolling as reported in Ref. [18,27,28]. Therefore, it is concluded that the β-phase stability is more effective than reduction ratio in developing rolling textures in β-type Ti-alloys.

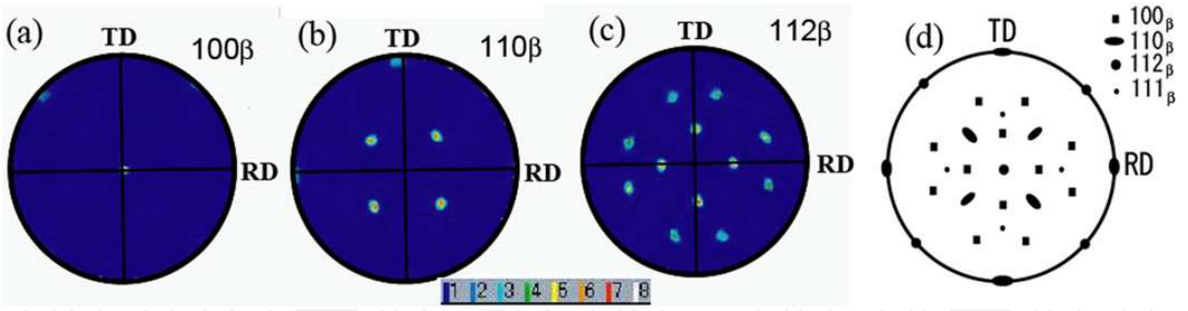


Figure 6. EBSD pole figures of alloy Z2 specimen after 90% cold rolling using 200_{β}, (a), 110_{β}, (b) and 112_{β} (c) and the stereoprojection of the $\{100\}_{\beta}<110>_{\beta}$-type texture, (d).

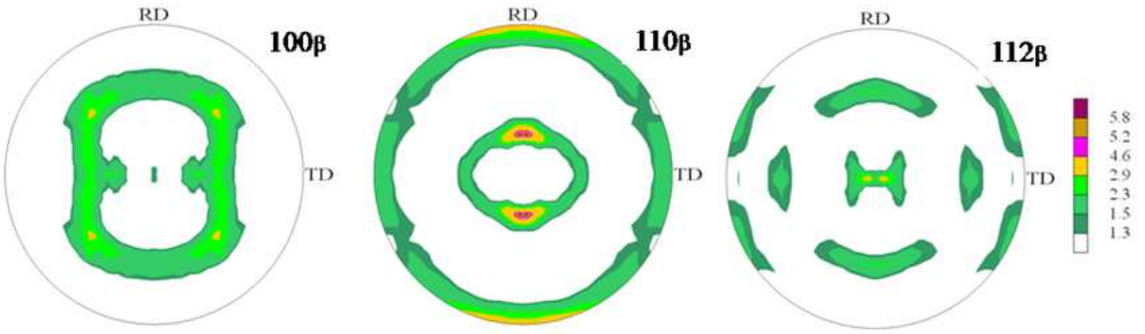


Figure 7. XRD pole figures of alloy A01 specimen after 98% cold rolling using 200β, 110β, and 112β.

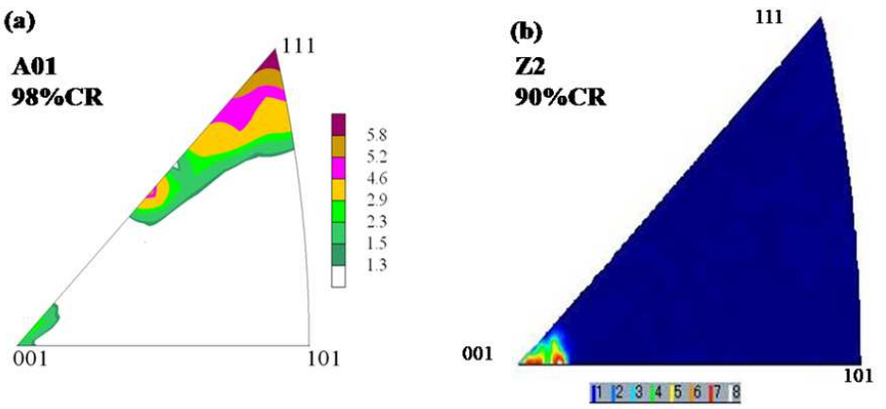


Figure 8. Inverse pole figures in the normal plane of alloy A01 specimen after 98% cold rolling calculated from the XRD ODF, (a), and alloy Z2 specimen after 90% cold rolling calculated from the EBSD ODF.

The β-type Ti-based alloys deform by either slip or twin mechanism [29,30]. The stress-induced martensitic transformation also takes place in some alloys upon applying external stress to them [30,31]. These phenomena emerge depending on the β-phase stability and

hence will be controlled by alloying. Also, it is known that the slip/twin boundary is close to the β/β+ω+(α") boundary [20].

As crystal deforms by slip, it undergoes crystal rotations. Such rotations lead to the development of preferred orientations in polycrystalline alloys [32]. The main reason why the {100}<110> texture develops by cold rolling in conventional bcc alloys may be attributable to the glide of dislocations along <111> on {011}, {112}or {123}[33] and the crystal rotations in them. It is well known that C' represents the resistance for the {011}<011> shear and C_{44} represents the resistance for the {001}<001> shear [34] and both of them decreases with decreasing β-phase stability [24,35]. The e/a value is kept at 4.24 in the present alloys and C' decreases with decreasing β-phase stability as discussed earlier, so the elastic softening will be enhanced in the order; Z1 < Z2 < Z 3 < Z4. This is a reason why the alloys locating at the β/β+α" boundary showed a very low shear modulus along both <011> on {011} and along <111> on {011}, {112} or {123} as reported in Ref. [36]. So it is expected that as the β-phase stability decreases, secondary slipping systems such as {011}<011> may be activated by deformation beside the main slipping system, i.e., <111> on {011}, {112}or {123}. As a result, a portion of the applied stress is consumed in slipping in such secondary slipping systems, which will make some disturbances in forming the main {100}<110> rolling texture. This can be a reason why the {100}<110> rolling texture was dominant in the high β-phase stability alloys. This was also seen in the steel in which the addition of a ferrite (bcc) stabilizer, Si, is enhanced to form the rolling texture [32].

4.3. Textures developed by recrystallization

The textures developed by severe cold rolling will diminish if the specimen is reheated for long time. For example, the $I_{H(cr)}$ of a 98%CR A01 specimen was decreased when reheated to different temperatures for 3 hrs, as shown in figure 9. $I_{H(cr)}$ is defined as $I_{Hcr}= 1/I_{Rcr}= I_{\{110\}\beta} / I_{\{200\}\beta}$. Hence, it is expected that the {100}<110> rolling texture is diminishing as a result of this reheating. The decrease in IH_{cr} was higher with increasing the reheating temperature till it reach a saturation temperature. This saturation temperature is most probably related to the completion of recrystallization process. Therefore, further increase in temperature will not affect much the value of IH_{cr}, as shown in figure 9. The rolling textures will not only diminish the heavily cold rolled specimens by reheating, but also recrystallization textures may develop as a result of this reheating.

In the present designed alloys, the recrystallization textures were developed in different strength in the ST specimen that was solution-treated after 90% cold rolling as explained bellow. In figure 4 (a) and table 2, the X-ray peak intensity and the intensity ratios are shown of the ST specimen solution-treated after 90% cold rolling. Here, $I_{Rst(1)}$ and $I_{Rst(2)}$ were defined as $I_{Rst(1)}= I_{\{110\}\beta} / I_{\{200\}\beta}$ and $I_{Rst(2)}= I_{\{211\}\beta} / I_{\{200\}\beta}$, respectively. Both of them decreased monotonously with increasing β-phase stability. Namely, in the recrystallization textures the high atomic density planes, i.e., {110} and {211}, aligned parallel to the rolling plane preferentially. This trend further increased with decreasing β- phase stability, as shown in table 2 for Z-alloys.

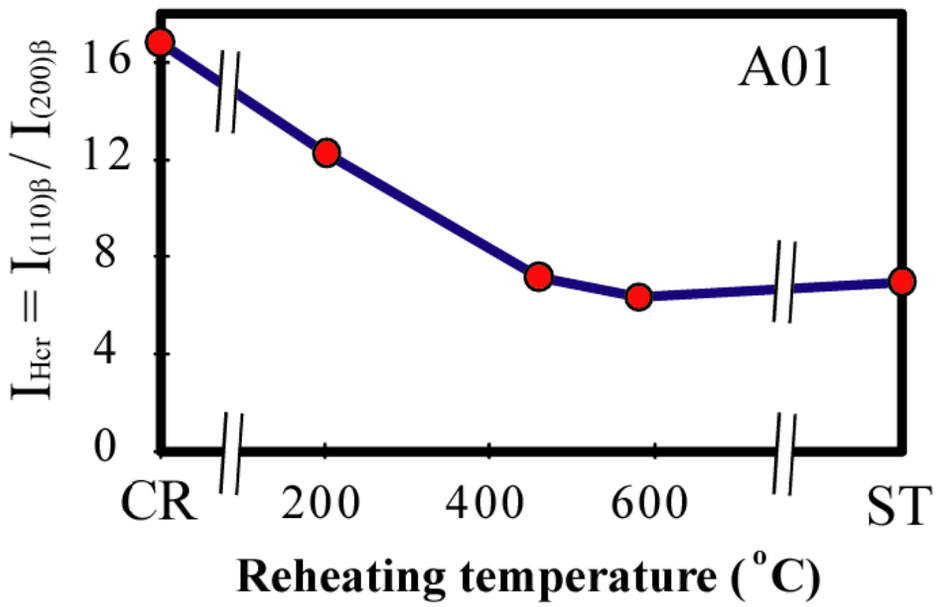


Figure 9. Effect of reheating temperature, for 3hrs, on the strength of formerly developed <100>{110} rolling texture after 98%CR, represented by *IHcr= 1/IRcr= I{110}▪ / I{200}▪* of the A01 alloy.

In figure 10, the EBSD Euler space plots are shown of the ST specimen of the alloys Z2-4 which were subjected to solution treatment at 1223K for 1.8 ks after 90% cold rolling. The Euler space density maps showed that the recrystallization textures were well developed in the alloy Z4, followed by the alloy Z3 and then the alloy Z2. Thus, the tendency of forming the recrystallization texture in the alloys changed in the order, Z4> Z3 > Z2, which was the opposite order of the rolling texture formed by cold rolling.

In the solution treatment after cold rolling, it has been reported that {112}<110> recrystallization texture is mainly developed in the low β-phase stability alloys such as Ti-24Nb-3Al alloy, position B in figure 3, [29,37] and Ti-35mass%Nb-4mass% Sn alloy, position A in figure 3, [31,38]. Beside this {112}<110> recrystallization texture, the {110}<211> texture is developed in a little higher β-phase stability alloy, Ti-35mass%Nb-7.9mass%Sn, position C in figure 3, [38]. However, only the {112}<110> recrystallization texture appears in the Ti-22Nb-6Ta alloy, position D in figure 3, [24]. It is important to note here that the {211}<110> recrystallization texture is well developed in the alloy only after severe cold rolling (i.e., 95% and 99%) [24,39] and it tends to diminish with decreasing reduction ratio of cold rolling [24]. Also, recrystallization textures could be controlled by the temperature and time for the heat treatment [39].

Recrystallization is the replacement of deformed grains by the recrystallized grains [40]. The grains with certain crystallographic orientations will be nucleated and grown in the course of annealing [41]. The growth rate of the grains is also 'oriented', because some grains with certain crystallographic orientation will grow faster than others [32]. Otherwise, 'oriented' nucleation may control the final texture structure. As discussed earlier, both the elastic softening and the elastic anisotropy becomes more remarkable with the

decrease in the β-phase stability. So, it was likely that the oriented nucleation and/or oriented growth was enhanced with decreasing β-phase stability, leading to the increase in the strength of the recrystallization texture.

From these discussions and the data given in table 2, it was concluded that, for the single β-phase alloys, the tendency of forming the {100}<110> texture by cold rolling increased with increasing β-phase stability, whereas, for low β-phase stability alloys (such as A00 and Z4 alloys in this study) other rolling textures may develop. On the other hand, the tendency of forming the recrystallization textures increased with decreasing β-phase stability. Thus, the β-phase stability was operating in the completely reverse way between the rolling and the recrystallization textures.

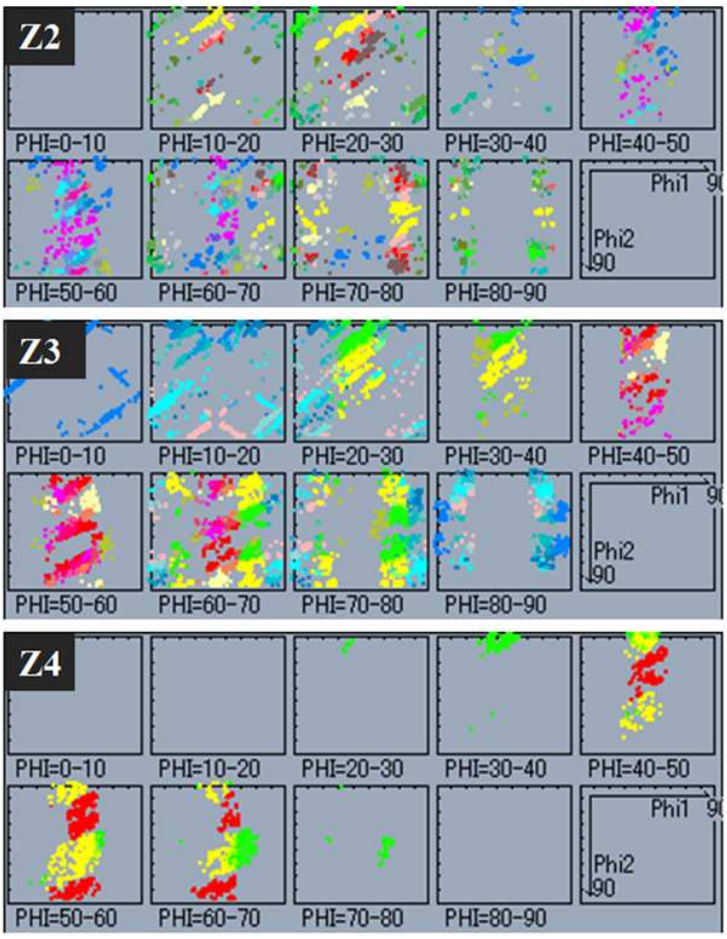


Figure 10. φ sections of the EBSD Euler space plot of alloys Z2-4 specimens solution treated at 1223K for 1.8 Ks after 90% cold rolling.

4.4. Textures developed in low β-phase stability alloys

The co-existence of α"- and/or ω-phase in the low β-phase stability alloys, such as Z4, A00 and A01 alloys in the present study, seems to affect much the deformation process and

therefore the rolling texture developed in them when severly deformed. This is because in such low β-phase stability alloys, the deformation by twin and/or stress-induced martensitic transformation mechanisms are predominant. The deformation stress are consumed in forming twinning and inducing ω and/or α" marensite phases. As a result, the grains rotation is expected to be much less in these low β-phase stability alloys resulting in low strength of the {100}<110> texture. For example, Z4 and A01 alloys show low I_{cr} and in the same time the stress induced α" martensitic transformation occurred in them by cold rolling, as evedinced from the two-steps yielding during the tensile test. For further details, refere to Refs. [25,42].

It is interesting to mention here that the low β-phase stability alloys, with α" martensite as the predominant phase, will show also a texture in the α"-phase, as shown in figure 11. The $\{200\}_{\alpha"}$, $\{012\}_{\alpha"}$ and $\{220\}_{\alpha"}$ XRD pole figures obtained from a 98%CR specimen of the low β-phase alloy,A00, are shown in Figure 11.a. The center of the pole figures corresponds to the direction normal to the specimen surface (ND). It seems from these pole figures that the α"-phase was textured in the specimen by cold rolling in the way that the $\{220\}_{\alpha"}$ planes aligned parallel to the rolling plane preferentially compared to the other textures and random grains orientations. In such low β-phase stability alloys, cold deformation induces aligned ω and/or α" martensite phases with orientation relationships as explained else where. The three α", ω, and β- phases are co-existed in A01 alloy after deformation as shown in figure 12. However, the ST specimen show less amount of α" martensite and the recrystalliztion texture in the α" –phase is also less as evidenced from figure 11.b for A00 alloy.

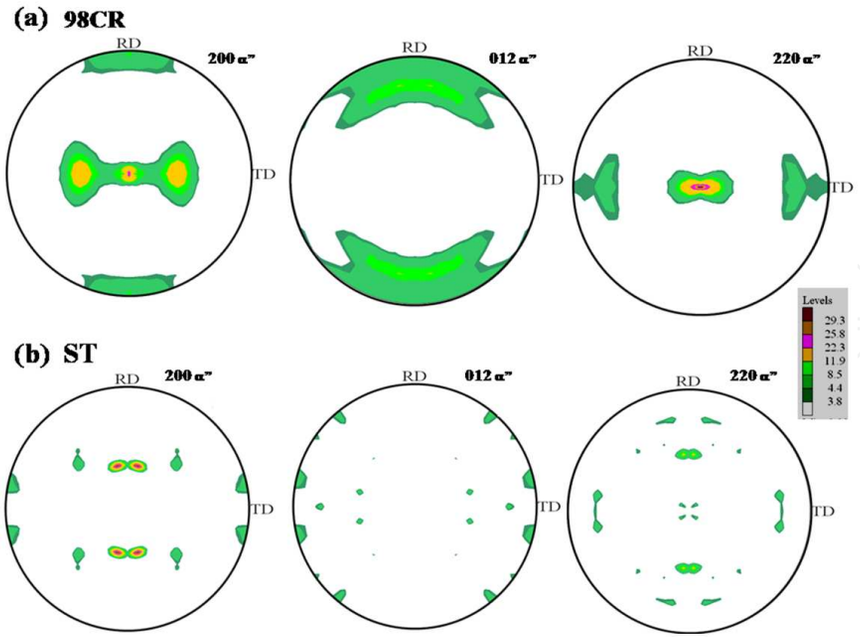


Figure 11. XRD pole figures of alloy A00 specimen after 98% cold rolling, (a) and after subsequent solution treatment at 1223K for 1.8 Ks, (b), using 200α", 012α", and 220 α".

http://dx.doi.org/10.5772/53588

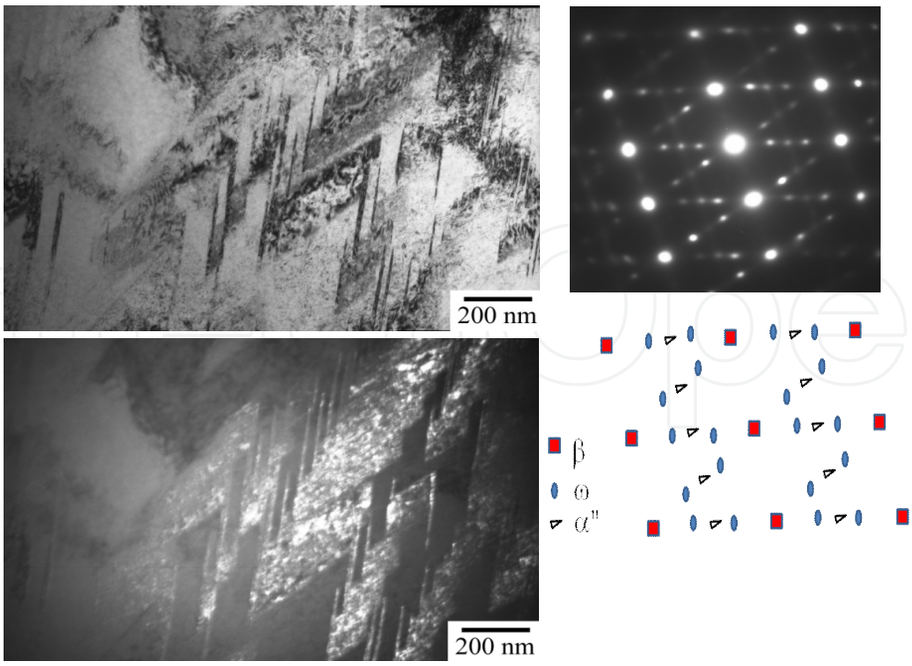


Figure 12. TEM analysis of a A01 specimen after 98CR. (a) and (b) present, respectively, bright-field and dark-field [imaged on $(-113)_\beta$] pair of micrographs showing stress induced of the ω and/or α"- phases; (c) shows the corresponding composite electron diffraction pattern and its key diagram. The ω-phase is with tow variants.

4.5. Microstructure change with β-phase stability

4.5.1. The microstructures after cold rolling

The microstructures shown in figure 13 are of the alloys Z2-4 after 90% cold rolled (90CR) in the RD and TD and the ND cross sections. The stream-like deformation bands were observed clearly along the RD and TD directions in both the RD and TD cross-sections. As the β-phase stability decreased, the deformation bands seemed to become finer. Also the density of the deformation bands seemed to be higher in the TD cross-section shown in figure 13.a than in the RD cross-section shown in figure 13.b.

The microstructure in an enlarged magnification is shown in figure 14 for the 90CR alloys. In the alloy 4, fine shear bands with an angle 42^O inclined to the main deformation band were observed in the RD cross-section. However, no such shear bands were observed in the TD cross-section. Also in the alloy Z3, the secondary finer deformation bands with the angles of 23^O and 37^O inclined to the main deformation bands were observed in the RD and TD cross-sections, respectively. Neither the shear bands nor the secondary deformation bands were observed in the alloy Z2 in both the RD and TD cross-sections. These results can be interpreted, as above, due to the presence of the texturing systems other than {100}<110> developed by the cold rolling and the plastic deformation among these three alloys depending on the β-phase stability. Also, the similarity in the TD and RD microstructure in the alloy Z2 is attributable to the well developed {100}<110> rolling texture in which both the RD and the TD are parallel to <110> [35].

4.5.2. The micorstructure after solution treatment

The microstructures of the ST alloys Z2-4 solution treated at 1223K for 1.8ks after 90% cold rolling are shown in figure 15. Shear bands supposedly provide the majority of nucleation sites during recrystallization in the severely cold rolled alloys. In particular, the triple joints between shear bands sites will work as nucleation sites [43]. So, the number of the nucleation sites was supposed to increase with decreasing β-phase stability, judging from the former deformation microstructures shown in figures 13 and 14. As a result, the grain size in the ST condition seems to decrease as the β-phase stability decreases. As is evident from the slightly defocused micrographs shown in figure 15.a some deformation bands still existed in the TD cross-section, although the recrystallization process seemed to be completed in the rolling plane shown in figure 15.b. However, the equiaxed grains were observed in the TD cross-section of the alloy Z2 in the ST condition in the EBSD image quality map (IQM) as presented in Ref. [25]. Similar deformation bands were observed in a Ti-45Nb alloy in the recrystallized condition after severe cold working [44]. The reason why these deformation bands still remained after the recrystallization treatment is not clear at the moment.

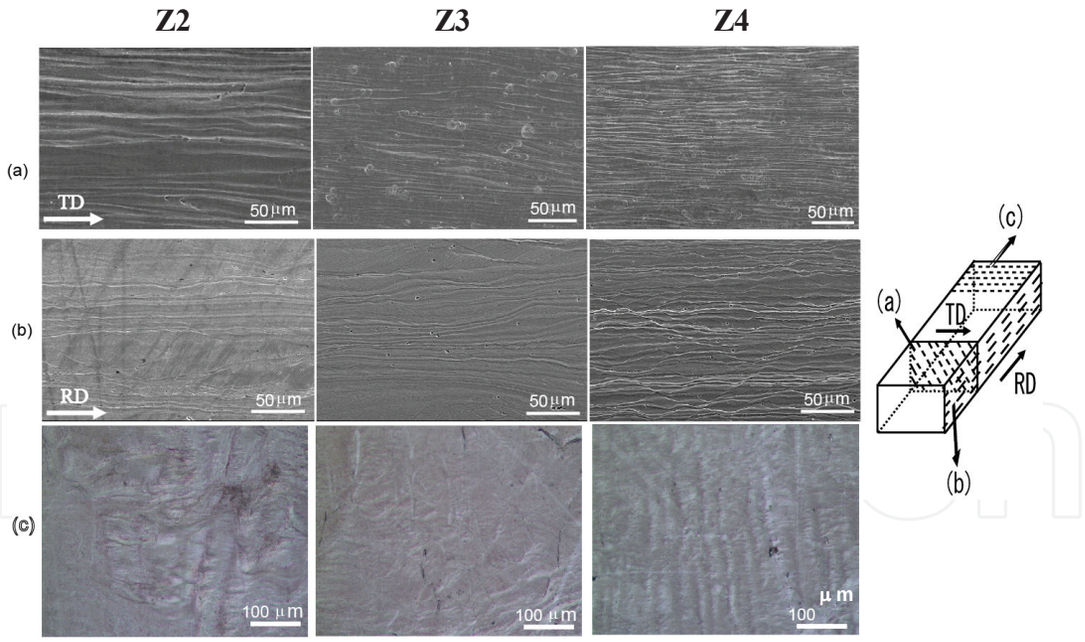


Figure 13. SEM micrographs of alloys Z2-4 after 90% cold rolling in the transverse, TD, cross-section (a), in the rolling, (RD), cross-section (b), and in the normal plane (c).

http://dx.doi.org/10.5772/53588

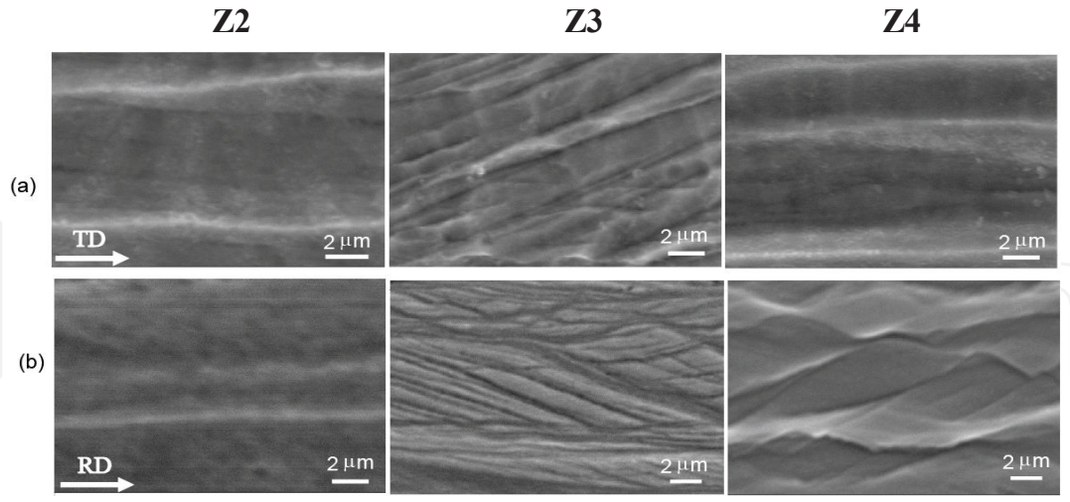


Figure 14. SEM micrographs of alloys Z2-4 shown in the enlarged scale of figure 13 (a) and (b).

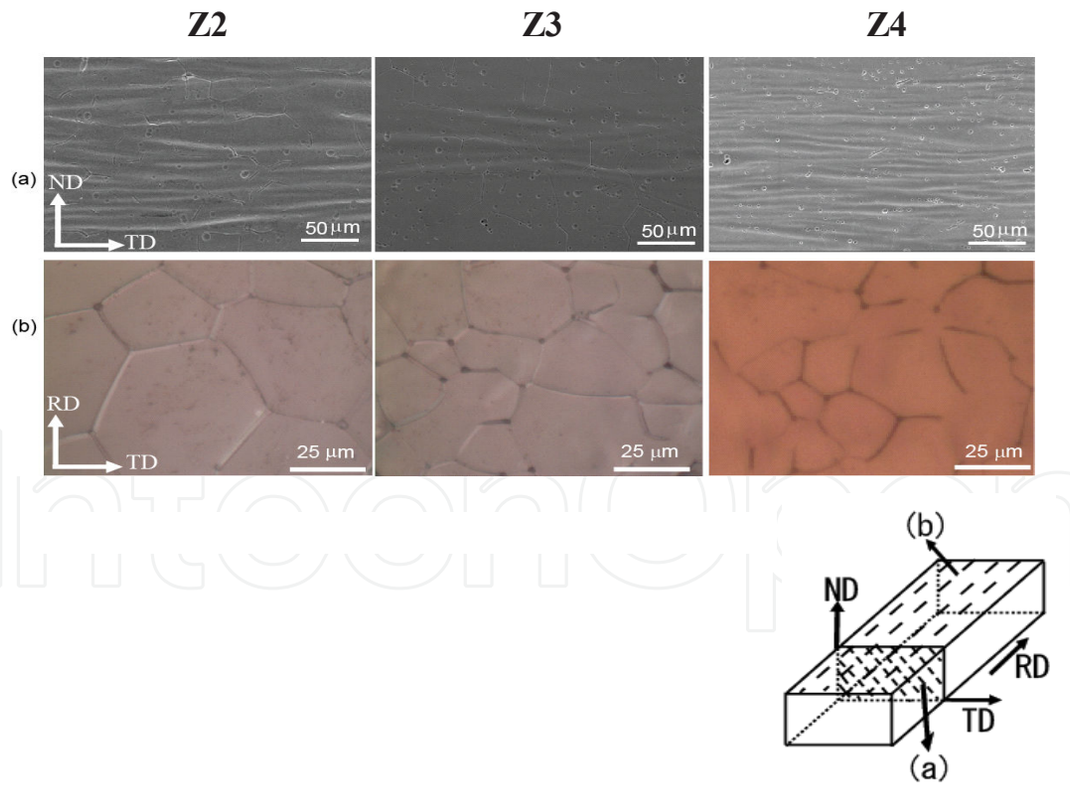


Figure 15. Micrographs of alloys Z2-4 after solution treatment at 1223K for 1.8 ks after 90% cold rolling in the transverse, TD, cross section, defocused SEM micrographs to show the deformation bands (a), and in the rolling plane, OM (b).

5. Conclusions

The $\overline{Bo}$-$\overline{Md}$ diagram was confirmed to be valid for the design of β-Type Ti alloys with irrelevant chemical compositions in the high $\overline{Bo}$ zone and with different β-phase stability. For the single β-phase alloys, the tendency of forming the {100}<110> texture by cold rolling increased with increasing β-phase stability, whereas, for low β-phase stability alloys (such as A00 and Z4 alloys in this study) other rolling textures may develop. On the contrary, the tendency of forming the recrystallization textures increased with decreasing β-phase stability and the recrystallization texture was more enhanced in the lower β-phase stability alloys resulting in the larger anisotropy of the properties.

Acknowledgments

The author thanks Prof. M. Morinaga of Nagoya University for his valuable comments and discussion, Prof. K. Sasaki of Nagoya University for his help with the TEM investigation, and Prof. H. Hosoda and Dr. T. Inamura of Tokyo Institute of Technology for their helpful discussions and XRD investigation. This study was supported by a Grant-in-Aid for Scientific Research from the Ministry of Education, Culture, Science, Sports and Culture of Japan, and by the Science and Technology Developing Fund (STDF) of Egypt.

Author details

Mohamed Abdel-Hady Gepreel

Department of Materials Science and Engineering, Egypt-Japan University of Science and Technology (E-JUST), Alexandria, Egypt

References

[1] H-R. Wenk, P.V. Houtte, Rep. Prog. Phys. 67 (2004) 1367.

[2] R. Sowerby, W. Johnson, Mater. Sci. Eng. 20 (1975) 101.

[3] M. Kawata, X-Ray analysis of residual stress and texture in ground carbon steels; Master theses; Toyohashi Univ. Tech., March (1982) pp. 45 and 47.

[4] E. Tenckhoff, A review of texture and texture formation in zircaloy tubing, Zirconium in the Nuclear Industry: Fifth Conference, ASTM STP 754 (1982) p. 5.

[5] J.C. Britt, K.L. Murty, Proceedings of Symposium (ZARC-91), BARC, Bombay (1991) p. 1.

[6] I.L. Dillamore, W.T. Roberts, Metals Reviews 10 (1965) 271.

[7] H.R Ogden, Ohio, in: Rare earth metals handbook, Physical properties of metals, C.A. Hampel (Edi), London, (1961), pp. 687-701.

[8] U.F. Kocks and H. Mecking, Prog. Mater. Sci. 48 (2003)171

[9] H. Honneff and H. Mecking, 6th Int. Conf. on Textures of Materials (Tokyo: The Iron and Steel Institute of Japan) (1981) p. 347.

[10] J.W. Christian, Proc. ICSMA 2: 2nd Int. Conf. on Strength of Metals and Alloys Vol. 1, ASM (1970) p. 29.

[11] Y.N. Wang, J.C.Huang, Mater. Chem. Phys. 81 (2003) 11.

[12] S.F. Castro, J.Gallego, F.J.G. Landgraf, H.J. Kestenbach, Mater. Sci. Eng. A 427 (2006) 301.

[13] K. Wierzbanowski, J. Tarasiuk, B. Bcroix, K. Sztwiertnia, P. Gerner, Recrystallization and grain growth, proceedings of the first joint international conference 12 (2000) 1075.

[14] S. Kuramoto, T. Furura, J.H. Hwand, K. Nishino, T. Saito, Metall. Mater. Trans. A 37 (2006) 657.

[15] S. Hanada, Sixth World Conf. on Titanium, France; Vol. 1 (1988) p. 105.

[16] S. Ankem, C.A. Greene, Mater. Sci. Eng. A 263 (1999) 127.

[17] S. Ishiyama, S. Hanada, O. Izumi, ISIJ Int. 31 (1991) 807–813.

[18] H. Matsumoto, S. Watanabe, S. Hanada, J. Alloys Compd. 439 (2007) 146–155.

[19] T. Saito, T. Furuta, J.H. Hwang, S. Kuramoto, K. Nishino, et al., Science 300 (2003) 464–467.

[20] M. Abdel-Hady, K. Henoshita, M. Morinaga, Scripta Mater. 55 (2006) 477–480.

[21] Y.N. Wang, J.C. Huang, Mater. Chem. Phys. 81 (2003) 11–26.

[22] M. Abdel-Hady, H. Fuwa, K. Henoshita, Y. Shinzato, M. Morinaga: Scripta. Mater. 57, 1000(2007).

[23] H. Ikehata, N. Nagasako, T. Furuta, A. Fukumoto, K. Miwa, T. Saito, Phys. Rev. B 70 (2004) 174113.

[24] E.S. Fisher, D. Dever, Acta Metall. 18 (1970) 265–269.

[25] M. Abdel-Hady, K. Henoshita, H. Fuwa, Y. Murata, M. Morinaga: Mater. Sci. Eng. A 480 (2008) 167.

[26] T. Inamura, Y. Fukui, H. Hosoda, S. Miyazaki, Mater. Sci. Forum. 475–479 (2005) 2323–2328.

[27] H.Y. Kim, T. Sasaki, H. Hosoda, S. Miyazaki, Acta Mater. 54 (2006) 423–433.

[28] H. Matsumoto, S. Watanabe, S. Hanada, Mater. Trans. 46 (2005)1070–1078.

[29] S. Ishiyama, S. Hanada, O. Izumi, ISIJ International 31 (1991) 807.

[30] W. Xu, K.B. Kim, J. Das, M. Calin, J. Eckert, Scripta Mater. 54 (2006) 1943.

[31] H. Matsumoto, S. Watanabe, S. Hanada, J. Alloy Compd. 439 (2006) 146.

[32] H.R. Wenk, P. Van Houtte, Rep. Prog. Phys. 67 (2004) 1368.

[33] T. Furuta, S. Kuramoto, J. Hwang, K. Nishino, T. Saito, Mater. Trans. 46 (2005) 3001.

[34] S. Kuramoto, T. Furura, J.H. Hwand, K. Nishino, T. Saito, Metall. Mater. Trans. A 37 (2006) 657.

[35] H.Y. Kim, T. Sasaki, H. Hosoda, S. Miyazaki, Acta Mater. 54 (2006) 423.

[36] T. Saito, T. Furuta, J. H. Hwang, S. Kuramoto, K. Nishino et al., Science 300 (2003) 464.

[37] T. Inamura, Y. Fukui, H. Hosoda, S. Miyazaki, Mater. Sci. Forum 475-479 (2005) 2323.

[38] H. Matsumoto, S. Watanabe, S. Hanada, Mater. Trans. 46 (2005) 1070.

[39] H. Hosoda, Y. Kinoshita, Y. Fukui, T.Inamura, M. Miyazaki, Mater. Sci. Eng. A 438-440 (2006) 870.

[40] Y.N. Wang, J.C. Huang, Mater. Chem. Phys. 81 (2003) 11.

[41] S.F. Castro, J. Gallego, F.J.G. Landgraf, H.J. Kestenbach, Mater. Sci. Eng. A 427 (2006) 301.

[42] M. A. Gepreel, Key Eng. Mater. 495 (2012) 62-66.

[43] O. Engler, Scripta Mater. 44 (2001) 229.

[44] Collings EW, Applied Superconductivity, Metallurgy and Physics of Titanium Alloys, Vol. 1. New York, Plenum Press (1986) pp. 464-469.

IntechOpen